We are IntechOpen, the world's leading publisher of Open Access books Built by scientists, for scientists

4,800
Open access books available

122,000
International authors and editors

135M
Downloads

Our authors are among the

154
Countries delivered to

TOP 1%
most cited scientists

12.2%
Contributors from top 500 universities

CLARIVATE ANALYTICS BOOK CITATION INDEX INDEXED

WEB OF SCIENCE™

Selection of our books indexed in the Book Citation Index in Web of Science™ Core Collection (BKCI)

Interested in publishing with us?
Contact book.department@intechopen.com

Numbers displayed above are based on latest data collected.
For more information visit www.intechopen.com

16

Vibration Measurement by Speckle Interferometry between High Spatial and High Temporal Resolution

Dan Nicolae Borza
Institut National des Sciences Appliquées de Rouen
France

1. Introduction

Speckle interferometry is a widely known successor of holographic interferometry. It is usually based on the use of a continuous wave laser. The use of temporal phase stepping allows obtaining the full-field of vibration amplitudes at the surface of the object under study. The simplest method is that of real-time, time-averaged speckle interferometry. It has been described for the first time in (Butters & Leendertz, 1971). The vibration amplitude map is usually presented as a two-dimensional fringe pattern, whose intensity modulation is given by the square of the Bessel function of the first kind and zero order whose argument is proportional with the local vibration amplitude. Roughly, the fringes are loci of points having the same vibration amplitude. The difference between the vibration amplitudes of points situated on adjacent fringes is close to a quarter of the laser light wavelength, which is something between 0.12 μm and 0.16 μm.

The most important general characteristics of this technique are justifying the interest in its use. It is a non-contact technique, so the object is not disturbed during the measurement. This is very important since there is no added mass or forces applied to the tested object, so its dynamic characteristics are not affected by the measurement process. It is a full-field technique, so there is no need to use many sensors or scan the surface in order to measure the vibration amplitudes of different points. All amplitudes are measured simultaneously. Finally, the sensitivity is very high and only small vibration amplitudes, up to a few micrometers, are necessary to produce the fringe pattern.

Along with these very favourable characteristics, a certain number of limitations also exist. The most obvious limitation is the noisy aspect of interferograms. Both additive and multiplicative speckle noise are affecting the interferograms. Further processing of the Bessel-type fringe patterns is difficult because of the speckle noise and of the weak contrast of successively increasing order fringes. As will be shown in this chapter, this task may become simpler by reducing the high-frequency multiplicative noise in the orthogonal components of the interferogram. Another limitation is related to the fact that the fringe pattern is obtained by integration, during the 3- or 4-frame bucket, of several cycles of vibration. During this time the vibration must be stationary and the temporal phase information related to the vibration is lost. In this chapter several advances in this field will be shown, allowing to make full-field measurements and resolve temporally the vibration.

2. Real-time, time-average speckle interferometry

The typical setup of a speckle interferometry vibration measurement system is shown in Fig. 1.

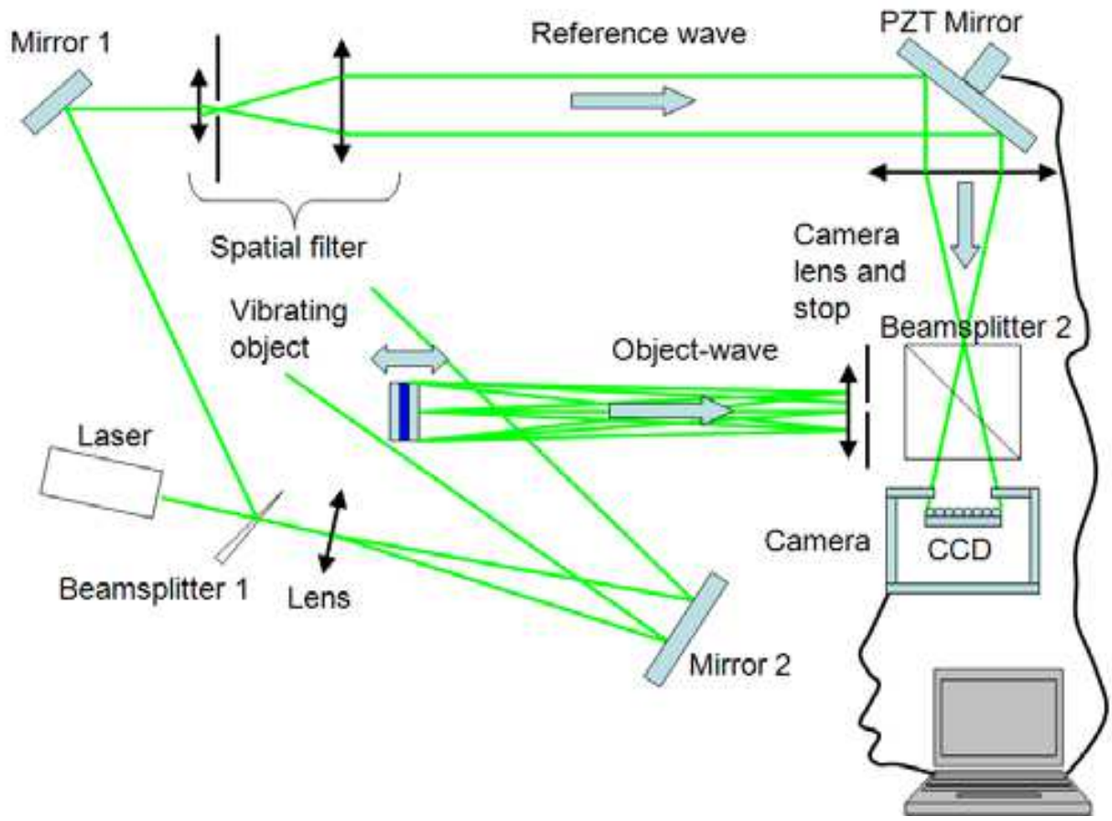

Fig. 1. Schematic lay-out of an out-of-plane sensitive time-average speckle interferometry system for vibrations

The vibrating object is illuminated by the CW laser beam transmitted by the beamsplitter, expanded by a lens and finally redirected by Mirror2 towards the vibrating object. The part of the laser beam reflected by the beamsplitter and by Mirror1 is expanded by a spatial filter and redirected, through the PZTMirror and the beamsplitter 2, towards the CCD detector. It is the reference beam. The PZT actuator placed behind PZTMirror is implementing the temporal phase stepping, producing a 4-step reference phase variation given by:

$$\Delta\varphi_i = (i-1)\frac{\pi}{2};\ i = 1,\ 2,\ 3,\ 4... \tag{1}$$

as first described in (Jbenathan, 1991).

In phase-stepped speckle interferometry, the raw data consist in number (usually 3 or 4) of correlograms recorded by the CCD detector. They represent the spatial sampling of the interference field between a uniform complex reference wave (usually of constant real amplitude R):

$$\bar{R} = R \cdot \exp\left[j\left(\varphi_r - \Delta\varphi_i\right)\right] \tag{2}$$

and a speckled object-wave

$$\begin{aligned}\bar{O} &= O \cdot \exp\left(j\varphi_o\right) = O \cdot \exp\left[j\left(\varphi_r + \varphi_{o-r} + \varphi_v \cos\omega t\right)\right] = \\ &= O \cdot \exp\left[j\left(\varphi_r + \varphi_{o-r}\right)\right] \cdot \exp\left[j\left(\varphi_v \cos\omega t\right)\right] = \bar{O}_0 \cdot \exp\left[j\left(\varphi_v \cos\omega t\right)\right]\end{aligned} \tag{3}$$

able to produce with the help of the camera lens a plane image of the harmonically vibrating object under study. The interference field of these waves is integrated by the camera during the frame acquisition time over an integer or large number of vibration periods. By putting $m = O^2 + R^2$ and $n = 2 \cdot O \cdot R$, the result may be described by the equation:

$$I_i = m + n\cos\left[\varphi_{o-r}\left(x,y\right) + \alpha\right] \cdot J_0\left[\varphi_v\left(x,y\right)\right] \tag{4}$$

In Eq. (2), $\varphi_{o\text{-}r}$ is the random phase difference between the uniform reference wave and the speckled object wave corresponding to a point *(x, y)* of the object in the equilibrium position. $J_0(\varphi_v)$ is the first kind, zero-th order Bessel function whose argument is the vibration-related phase given by the approximate relation:

$$\varphi_v\left(x,y\right) = \frac{4\pi}{\lambda} d\left(x,y\right) \tag{5}$$

where *d* is the vibration amplitude of the *(x, y)* point. In any speckle interferometry system based on 4-frame buckets (Creath, 1985), the four phase-stepped data fields given by Eq. (1) are used to calculate (either in real-time or during post-processing) the differences:

$$C = I_1 - I_3 = 2OR\cos\phi_{o-r} \cdot J_0\left(\varphi_v\right) \tag{6}$$

and:

$$S = I_4 - I_2 = 2OR\sin\varphi_{o-r} \cdot J_0\left(\varphi_v\right) \tag{7}$$

These two orthogonal data fields (Borza, 2004) may be used to compute and display the usual time-averaged fringe pattern:

$$I_{TAV} = \sqrt{S^2 + C^2} = 2OR\left|J_0\left[\varphi_v\left(x,y\right)\right]\right| \tag{8}$$

They may also be considered as the real and imaginary components, in the detector plane, of a reconstructed complex wave (A is a constant):

$$\bar{O}_R = A \cdot O \cdot J_0\left[\varphi_v\left(x,y\right)\right]\exp\left(j\varphi_{o-r}\right) \tag{9}$$

One should be aware that any individual frame or the corresponding data fields or the interferogram itself are time-averaged, even if, as a particular case, the object is immobile during the integration time. In this case, Eq. (9) simply becomes:

$$\bar{O}_R = A \cdot O \cdot \exp\left(j\varphi_{o-r}\right) \tag{10}$$

The maxima (bright fringes) of Eq. (8) correspond to vibration amplitudes of 0 (zero) - for the brightest fringes showing the nodal lines, then to amplitudes of

$$d = (k + \frac{1}{2}) \cdot \frac{\lambda}{4} \text{ (k=1, 2, 3 ...)} \quad (11)$$

The minima (dark fringes) correspond to amplitudes:

$$d = k \cdot \frac{\lambda}{4} \quad (k = 1,\ 2,\ 3 \ldots) \quad (12)$$

The typical aspect of time-averaged fringes seen either in real-time on the monitor while looking at a vibrating object, or saved on the disk, is shown in Fig. 2 (Nistea & Borza, 2010a).

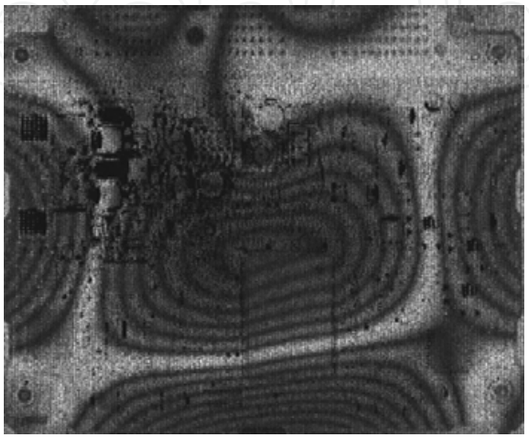

Fig. 2. Time-averaged speckle interferogram of an electronic assembled microcontroller card excited at one of its resonance frequencies at 841 Hz

It corresponds to a vibration during which the object reaches periodically the position of extreme deflection with regard to the equilibrium position, as shown in Fig. 3.

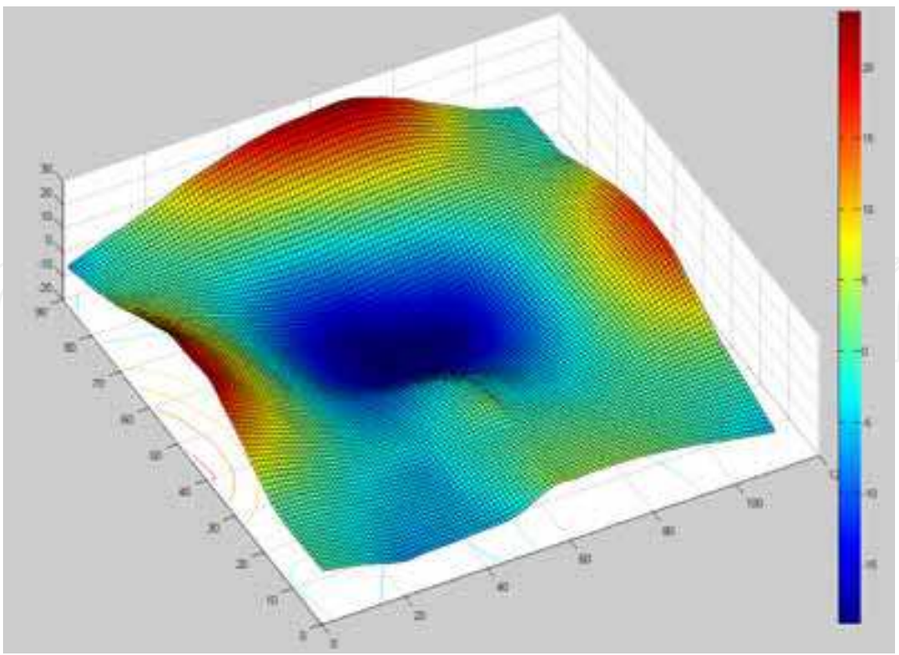

Fig. 3. Vibration amplitude-related phase map corresponding to interferogram in Fig. 2. Values are in radians.

The interferograms obtained by this method are also called *electronic holograms*, or, when it's no possibility of confusion with a "classical" hologram obtained through diffraction of the reference beam by the primary fringes recorded on photorecording media, simply *holograms*. To adress one of the limitations already mentioned for the time-average method, the speckle noise, one may record several time-average interferograms and eventually rotate the object illumination beam between recordings. By averaging a number of N interferograms, the speckle noise is reduced by $\sqrt{N}$, as shown in Fig. 4

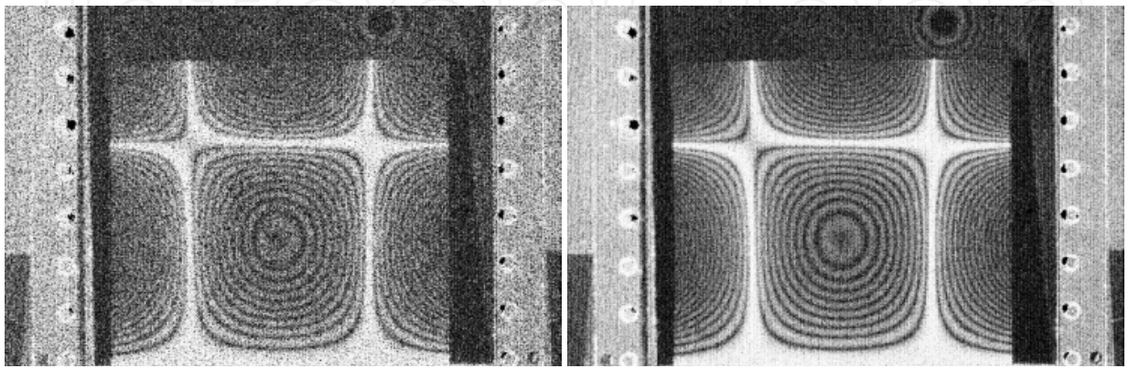

Fig. 4. Time-averaged holograms of a vibrating plane plate: at left a single hologram, at right the result of four hologram averaging.

Filtering a time-averaged hologram by convolution with an average or other low-pass filter may reduce the high-frequency noise, but strongly affects the fringe resolution and contrast.

3. Development of speckle interferometry vibration measurement methods

3.1 Reference wave modulation

One of the well-known drawbacks of time-average holograms is the impossibility to obtain by an automatic procedure the explicit full-field of vibration amplitudes. This problem was adressed (Pryputniewicz & Stetson, 1999) by using the reference wave homodyne modulation, in order to record several fringe patterns spatially shifted. Through the use of look-up tables, the final result is a wrapped amplitude-related phase fringe pattern. Such a fringe pattern is shown in Fig. 5.

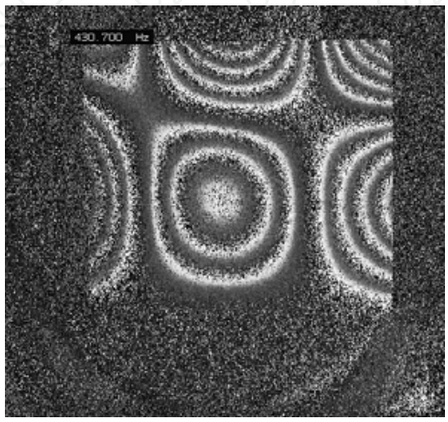

Fig. 5. Phase image of the vibration mode presented in Fig. 4.

The introduction of the homodyne modulation of the reference wave thus allows using slightly modified 2d unwrapping procedures in order to unwrap the fringe pattern and obtain the explicit amplitude map.
The method works well, but from the practical point of view is rather cumbersome as it implies changing several times the amplitude and the phase of the exciting voltages applied to the object and to the modulating mirror.
Other authors described the possible use of heterodyne phase modulation in time-average speckle interferometry. In (Høgmoen and Løkberg, 1977) this type of modulation is used to allow measurement of very small vibration amplitudes.

3.2 Stroboscopic principles

Apart from the methods based on the modulation of the reference wave, the only possibility to obtain phase fringe patterns for vibrating objects is to avoid the temporal averaging, or the integration during the recording of a frame. It means the CCD exposure should be much smaller than the period of vibration. This may be achieved by using stroboscopic principles or pulsed lasers. Several researchers studied the application of stroboscopic techniques to speckle interferometry. Stroboscopic techniques are "freezing" the vibration for the moments when data are recorded, like speckle interferometry with pulsed lasers. The correlograms recorded, which are the primary data fields from which interferograms are computed, are related only to certain well-defined positions. The temporal integration thus disappears, and so does the Bessel-type fringe profile. The simplest interferometric reconstructions are double-exposure holograms rather than time-averaged. The use of these techniques allows, as described in (Valera et al, 1997), the study of objects which are vibrating simultaneously at two frequencies whose ratio is an irrational number. The separation of the two vibration modes is made by stroboscopic heterodyned speckle interferometry. By choosing the frequency of the strobing pulses equal with one of the two frequencies of vibration, only the vibration of the second frequency was measured by the interferogram.
Stroboscopic techniques may also be used for measuring the response of a structure both in phase and in quadrature with the exciting force, allowing thus (Van der Auweraer et al, 2002) to estimate the real part and the imaginary part of the response of the object. This is an important step in experimental modal analysis.
Many other methods and two excellent reviews of the state-of-the-art were published by (Doval, 2000; Jacquot, 2008).

4. Vibration measurement with high spatial resolution

Several researchers proposed different experimental methods and algorithms based on the joint use of correlograms recorded with the object at rest and during vibration.
(Wang et al, 1996) made a thoroughful analysis of three methods based on the addition or subtraction of video signals recorded in such situations. For the particular case of the amplitude-fluctuation method, the subtraction between the signals corresponding to two different signals during vibration is shown to produce fringes dependent on the Bessel function $J_1[\varphi_v(x,y)]$ instead of $J_0[\varphi_v(x,y)]$. The subtraction of the speckled image of an object from that of the object at rest, as in (Nakadate, 1980), produces a fringe pattern given by:

$$I = 1 - 2 \cdot J_0(\varphi_v) \cdot [\cos(\varphi_{stat})] + J_0^2(\varphi_v) \tag{13}$$

If the speckle decorrelations are kept to a reasonable level, they might be approximated by:

$$I = [1 - J_0(\varphi_v)]^2 \tag{14}$$

As underlined in (Creath & Slettemoen, 1985) this type of fringes are equivalent to those appearing in real-time holographic interferometry. Their contrast is lower compared to time-average fringes, but they offer a valuable tool in studying vibrations of very small amplitudes.

In order to analyze the possibilities for reducing the speckle noise of the time-averaged speckle interferograms and advance towards high spatial resolution, one has to look at the expression of one of the correlograms recorded in the original 4-frame bucket. It is given by Eq. (4). In the expression $m + n\cos[\varphi_{o-r}(x,y) + \alpha] \cdot J_0[\varphi_v(x,y)]$, m (the bias) denotes the sum between the speckled image of the object and the uniform intensity of the reference beam, so it represents additive noise. The variable n (the modulation) denotes the square root of the product of the same terms (the speckled image of the object and the uniform intensity of the reference beam). This noisy term is multiplied by $\varphi_{o-r}(x,y)$ which is the random phase difference, of very high spatial frequency, between the object wave and the reference wave. The last factor of the product, $J_0(\varphi_v)$, is the only deterministic factor; the argument of the Bessel function is the spatial phase introduced by the object vibration. Unfortunately, with the exception of the nodal points where $\varphi_v = 0$ and $J_0(\varphi_v) = 1$, the product $n \cdot \varphi_{o-r}(x,y) \cdot J_0(\varphi_v)$ is dominated by the multiplicative speckle noise and the Bessel function is deeply covered by noise.

In the (usual) case of 4-frame correlogram buckets of vibrating objects, the additive noise is eliminated, as shown by Eq. (6) and (7), by making the differences between the frames phase-shifted by π. In the remaining expressions, $C = 2 \cdot O \cdot R \cdot \cos(\varphi_{o-r}) \cdot J_0(\varphi_v)$ and $S = 2 \cdot O \cdot R \cdot \sin(\varphi_{o-r}) \cdot J_0(\varphi_v)$ the multiplicative noise is still there. Any attempt to apply a low-pass filter to these two orthogonal components of the time-averaged hologram would "spread" the high-frequency noise and make impossible the interferogram reconstruction. To compensate the speckle noise we can use the similar terms from another 4-frame bucket, or, better, from a 4-frame bucket during which the object was at rest. Assuming that speckles didn't decorrelate between the acquisition of the frames with the object at rest and the acquisition with the vibrating object, but admitting a small phase difference $\Delta\varphi_{o-r}$, which may have as origine, for example, a small displacement or a thermal drift, these terms have the expressions:

$$J_i = m + n\cos\left[\varphi_{o-r}(x,y) + \Delta\varphi_{o-r} + \alpha\right] \tag{15}$$

and they are used to compute:

$$C' = J_1 - J_3 = 2OR\cos\left(\varphi_{o-r} + \Delta\varphi_{o-r}\right) \tag{16}$$

and

$$S' = J_4 - J_2 = 2OR\sin\left(\varphi_{o-r} + \Delta\varphi_{o-r}\right) \tag{17}$$

Eqs. (6), (7), (16) and (17) may be used to compute:

$$S_0 = S \cdot C' - S' \cdot C = 4O^2R^2 \cdot J_0(\varphi_v) \cdot \sin(\Delta\varphi_{o-r}) \tag{18}$$

and

$$C_0 = S \cdot S' + C' \cdot C = 4O^2R^2 \cdot J_0(\varphi_v) \cdot \cos(\Delta\varphi_{o-r}) \tag{19}$$

The data fields described by Eqs. (18) and (19) are important because they are almost noise-free; the high-frequency multiplicative speckle noise has been eliminated.
As described in (Borza, 2000; Borza, 2002; Borza, 2005) the two quadrature data fields may be used for hologram restoration by a procedure equivalent to the synchronous detection. Eqs. (18) and (19) allow computing the phase difference by using the arctangent function, $\tan^{-1}(S_0 / C_0)$.
If the 4-quadrant arctangent function is used instead, the sign of the numerator and of the denominator are evaluated separately and the result goes in the right quadrant. Then the identical factors in these expressions, $4 \cdot O^2 \cdot R^2 \cdot J_0(\varphi_v)$, will disappear, with one particular remark. The quadrant where the angle will be placed depends on the sign of the Bessel function $J_0(\varphi_v)$. Each time this factor will change its sign, the result

$$I_{ph} = a\tan 2\left(\frac{S_0}{C_0}\right) = \Delta\varphi_{o-r} \cdot \mathrm{sgn}\left[J_0(\Delta\varphi_{o-r})\right] \tag{20}$$

will also change sign. If the phase difference between the object at rest and the mean position of the vibrating object is close to zero, the fringe pattern is a quasi-binary one, as in fig. 6.

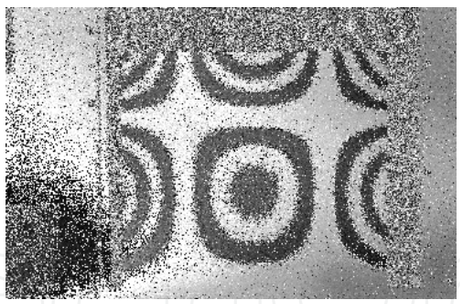

Fig. 6. Quasi-binary fringe pattern

This kind of "quasi-binary" fringes have also been reported by other authors (Picart et al, 2005; Singh et al, 2007).
Since the two orthogonal data fields are noise-free, the whole process may be described by the classical description of synchronous detection, as in fig. 7.
The two noise-free data fields may be low-pass filtered and the resulting quasi-binary hologram, showing the sign of the Bessel function (fig. 8a) may be the starting point for a procedure aiming at the obtention of the explicit vibration amplitude map.
Even more important is the reconstruction of the time-averaged hologram presented in fig. 8b. This becomes possible with the help of the filtered orthogonal components. It is a high spatial resolution hologram, allowing to determine the positions of the zeroes of the Bessel dark fringes in subpixel resolution.

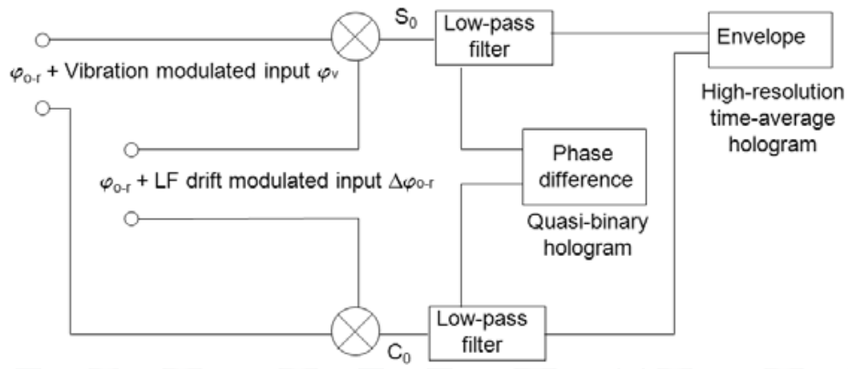

Fig. 7. Principle of synchronous detection.

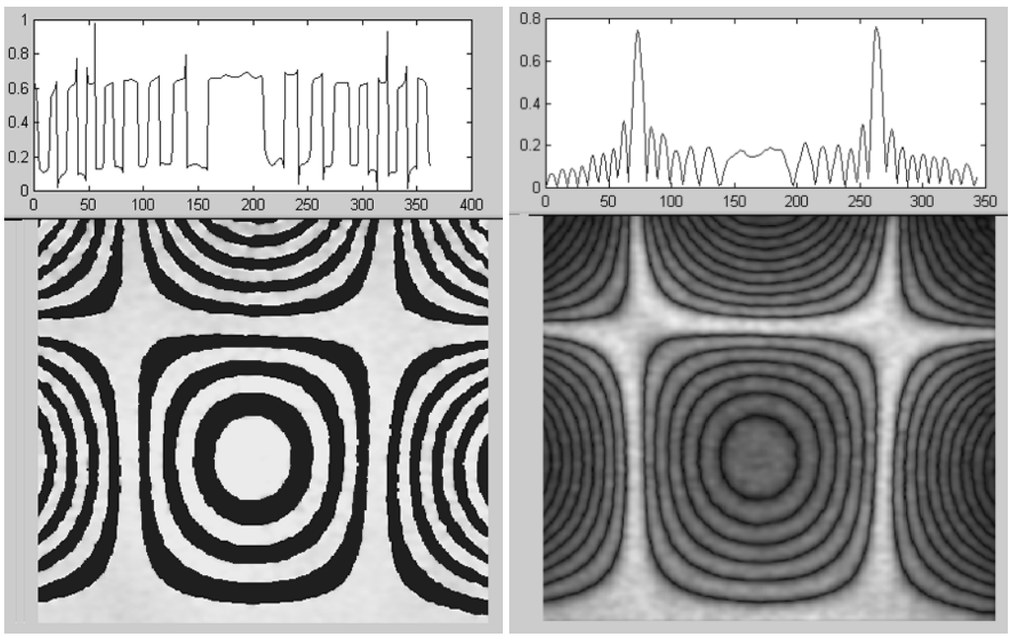

a b

Fig. 8. (a) Quasi-binary hologram after filtering its orthogonal components; profile grey values are normalized between 0 and 1; (b) high spatial resolution time-average hologram

The paper (Borza, 2006) describes a method, having as starting point this kind of high-resolution time-average hologram, for automatically indexing in subpixel resolution all the dark and bright fringes and then obtaining the vibration amplitude in each point by simply inverting the Bessel function on its monotonicity intervals (fig. 9).

5. A unifying approach for speckle noise reduction in vibration measurement by high resolution time-average speckle interferometry

Since the methods presented in the last Section are using the phase difference between the states with the object at rest and with the object in vibration, and the eventual static deformation (described by $\Delta\varphi_{o-r}$) between these two instants has been taken into account in Eq. (15) and the following, it is reasonable to try doing a more systematic description in a unifying approach.

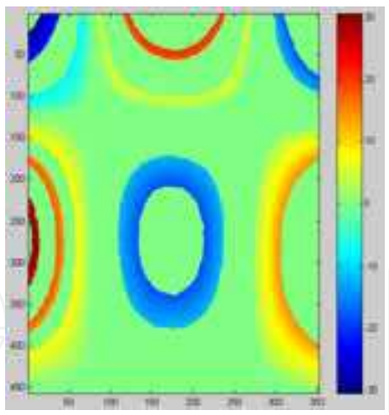

Fig. 9. Partially unwrapped vibration map by regional inverting of the Bessel function

In the most general situation, the two object states which are compared in the final interferogram may be characterized by:

- The first state: the object in vibration, described by the vibration-related phase φ_{v1};
- The second state: the object deformed (or displaced statically), as described by $\Delta\varphi_{o-r}$ and having also a second vibration, described by the vibration-related phase φ_{v2}.

In this case, for the first state the two orthogonal data fields computed from the 4-frame buckets acquired are:

$$\begin{aligned} C_{v1} &= A \cdot O \cdot J_0(\varphi_{v1}) \cdot \cos\varphi_{o-r} \\ S_{v1} &= A \cdot O \cdot J_0(\varphi_{v1}) \cdot \sin\varphi_{o-r} \end{aligned} \tag{21}$$

and:

$$\begin{aligned} C_{v2} &= A \cdot O \cdot \cos(\varphi_{o-r} + \Delta\varphi_{o-r}) \cdot J_0(\varphi_{v2}) \\ S_{v2} &= A \cdot O \cdot \sin(\varphi_{o-r} + \Delta\varphi_{o-r}) \cdot J_0(\varphi_{v2}) \end{aligned} \tag{22}$$

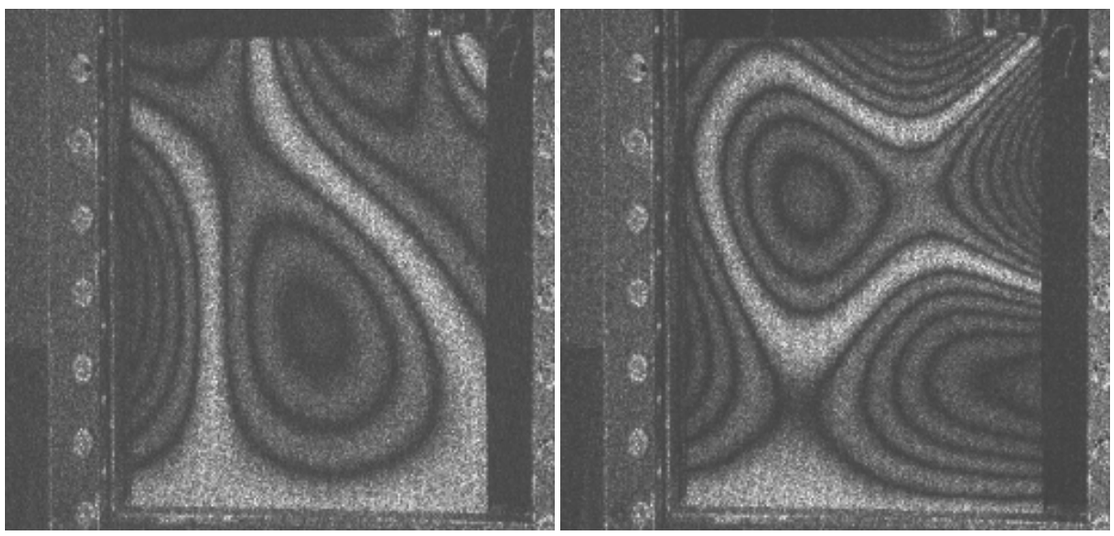

Fig. 10. Time-averaged holograms corresponding to the 2 vibration states.

In both cases, the time-averaged holograms obtained by eq. (8) are showing (fig. 10) Bessel-type fringe patterns which are related only to the vibration-related phase, either φ_{v1} or φ_{v2}.

$$I_{TAV1} = \sqrt{S^2 + C^2} = 2OR\left|J_0\left[\varphi_{v1}(x,y)\right]\right| \tag{23}$$

$$I_{TAV2} = \sqrt{S^2 + C^2} = 2OR\left|J_0\left[\varphi_{v2}(x,y)\right]\right| \tag{24}$$

Several situations may be imagined when combining the data fields from the two object states.

5.1 Phase difference of data fields - General case

The two orthogonal data fields which may be calculated from Eqs. (21) and (22) by using the formulæ:

$$\begin{aligned} S &= S_{v1}C_{v2} - C_{v1}S_{v2} \\ C &= C_{v1}C_{v2} + S_{v1}S_{v2} \end{aligned} \tag{25}$$

are given by the expressions:

$$\begin{aligned} S &= A^2O^2J_0(\varphi_{v1})J_0(\varphi_{v2})\sin\Delta\varphi_{o-r} \\ C &= A^2O^2J_0(\varphi_{v1})J_0(\varphi_{v2})\cos\Delta\varphi_{o-r} \end{aligned} \tag{26}$$

The square root of the sum of their squares is expressed by the absolute value of the product of the two Bessel functions:

$$I_{TAV12} = I_O \cdot \left|J_0(\varphi_{v1}) \cdot J_0(\varphi_{v2})\right| \tag{27}$$

and their relative phase is:

$$\Delta\varphi_{12} = \Delta\varphi_{o-r}\,\mathrm{sgn}\left[J_0(\varphi_{v1}) \cdot J_0(\varphi_{v2})\right] \tag{28}$$

They are illustrated in fig. 11.

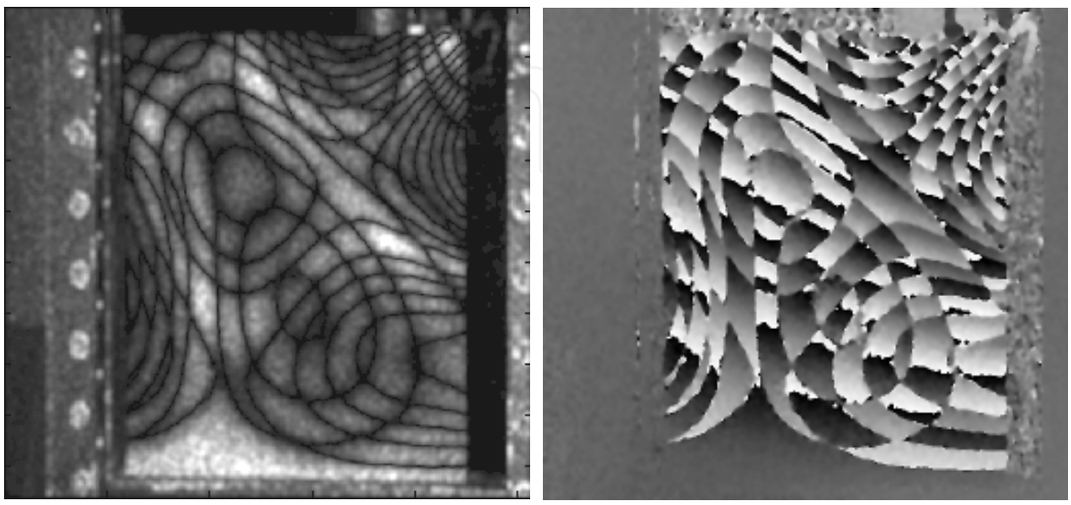

Fig. 11. Fringe patterns corresponding to Eqs. (27) and (28)

The static term, $\Delta\varphi_{o-r}$, may be caused by different phenomena: sometimes it appears because of air turbulences or thermal gradients between the two series of exposures, sometimes it reflects variations of the optical path in the object-wave due to a mechanical movement or the object deformation between the two recordings. If $\Delta\varphi_{o-r}$ is not too large, it may be easily compensated by post treatment of data (fig. 12).

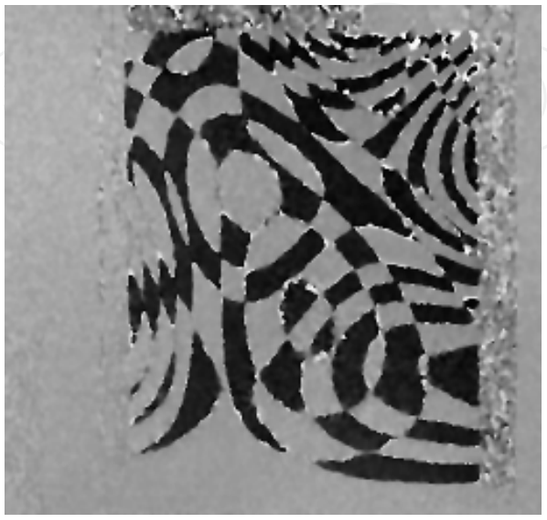

Fig. 12. Phase difference with compensated $\Delta\varphi_{o-r}$

5.2 Phase difference in a particular case: object at rest in the first state

This is the most current case; if during the second state there is no static phase difference with respect to the first state, one retrieves the situation already described in § 4. If the static phase difference is not negligible, then the phase difference is given by eq. (20) and shown in fig. 13..

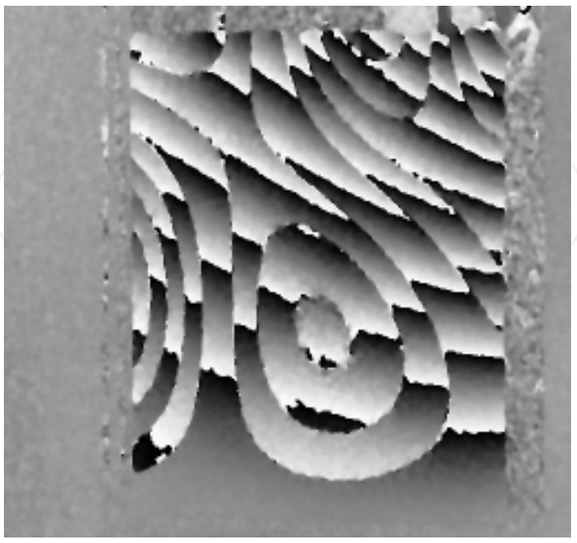

Fig. 13. Quasi-binary hologram with an important static phase difference and vibration of the object in one of the two states.

To fully appreciate the spatial resolution gain of time-average speckle interferometry when using the presented method, fig. 14 illustrates the usual time-average hologram and the high-resolution one, recorded during the same experience, along with the profiles across fringes. The values on the scales of grey levels are conventional values obtained by two different normalizations.

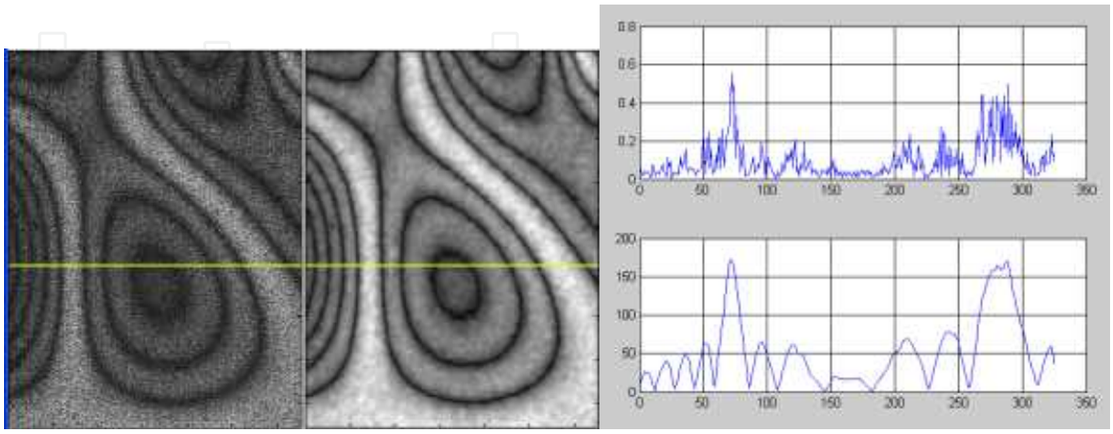

Fig. 14. Time-average (left), high resolution time-average (middle) interferograms and profiles across the fringe patterns (right)

5.3 Phase difference in a particular case: object vibrating identically in both states

The vibration amplitude and phase being identical in both states, $\varphi_{v1} = \varphi_{v2}$. In this case eq. (21) is replaced by:

$$\begin{aligned} C_{v1} &= C_{v2} = A \cdot O \cdot J_0(\varphi_{v1}) \cdot \cos\varphi_{o-r} \\ S_{v1} &= S_{v2} = A \cdot O \cdot J_0(\varphi_{v1}) \cdot \sin\varphi_{o-r} \end{aligned} \tag{29}$$

Eq. (25) become:

$$\begin{aligned} S &= S_{v1}C_{v1} - C_{v1}S_{v1} = A^2O^2J_0^2(\varphi_{v1}) \cdot \sin(\Delta\varphi_{o-r}) \\ C &= {C_{v1}}^2 + {S_{v1}}^2 = A^2O^2J_0^2(\varphi_{v1}) \cdot \cos(\Delta\varphi_{o-r}) \end{aligned} \tag{30}$$

Equation (28) becomes:

$$\Delta\varphi_{12} = \Delta\varphi_{o-r}\,\mathrm{sgn}\left[J_0^2(\varphi_{v1})\right] = \Delta\varphi_{o-r}\big|_{\mathrm{mod}\,2\pi} \tag{31}$$

This result is shown in fig.15.
The detailed explanations for this kind of fringe patterns are found in (Borza, 2008).

6. Speckle interferometry with high temporal resolution

The spatial resolution of speckle interferometry is in most cases high enough for the needs of the measurements, and the vibration amplitude maps found by this technique are used, as in (Moreau, 2008) to check and validate the results produced by other techniques (Laser Doppler Velocimetry, Near-Field Acoustical Holography).

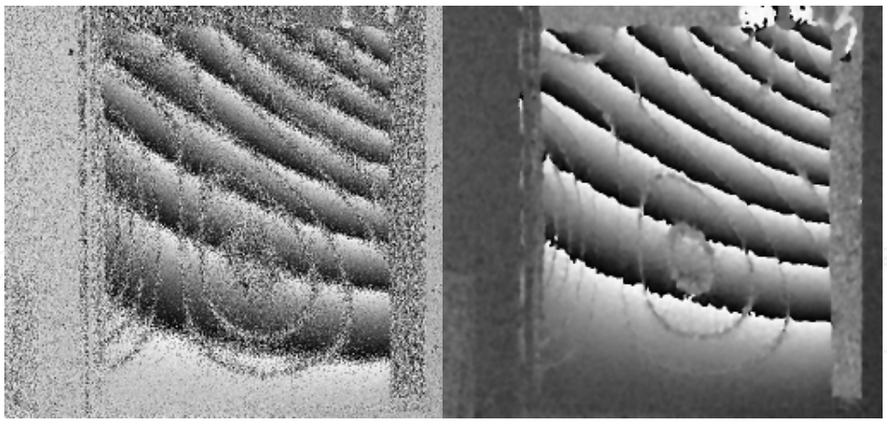

Fig. 15. Non-filtered (left) and filtered (right) patterns showing the static phase difference between two vibrating states of the object

The direction into which speckle interferometry should make the bigger steps is improving its temporal resolution, so as to be able to characterize the relative vibration phase between different points, the vibration waveform, or to cope with non-stationary phenomena.
The use of the pulsed laser is partially a solution, but the costs and technical difficulties are high, and the repetition rate of laser pulses rather limited.
The development of high-rate digital cameras and the increasing data transfer speed between such devices, memory and disk units in computers encouraged an increasing numer of researchers to work in speckle interferometry with high rate cameras.
Different systems and specific problems have been described in the litterature, allowing to appreciate that speckle interferometry is more and more able to study dynamic and non-periodic deformations with a good temporal resolution.
In (Aguanno et al, 2003) is presented the Single Pixel Carrier Based Demodulation approach with a digital CMOS-DSP camera for full-field heterodyne interferometry. The result is a full-field vibration measurement system able to operate, without scanning, like a classical scanning Laser Doppler Vibrometer (LDV). In (Asundi & Singh, 2006; Kaufmann, 2003) are presented the possibilities of dynamic digital holography, respectively dynamic speckle interferometry to measure amplitude and phase.
(Nistea & Borza, 2010b) presented a speckle interferometry system based on a use of a high-rate, low-cost CMOS camera and some of their work with this system. The measurement system uses a 300 mW CW Nd-YAG laser. It may be configured to work with or without temporal phase stepping. If used, phase stepping is implemented by an acousto-optic phase modulator. Some of the results obtained with this system are described in the next sections.

6.1 Object submitted to a mechanical shock: free oscillations, no phase stepping

The measurements of a small plate clamped along the left side (fig. 16) submitted to a shock were made by acquiring at the rate of 15600 frames/ second, without phase stepping, correlograms having the dimension 118 x 39 pixels. The temporal history of any pixel contains 21840 points. For a randomly chosen pixel, marked with a cross in fig. 16, it is possible to determine the amplitude at any moment, the free oscillation frequency, the eventual delays between pixels and the damping.

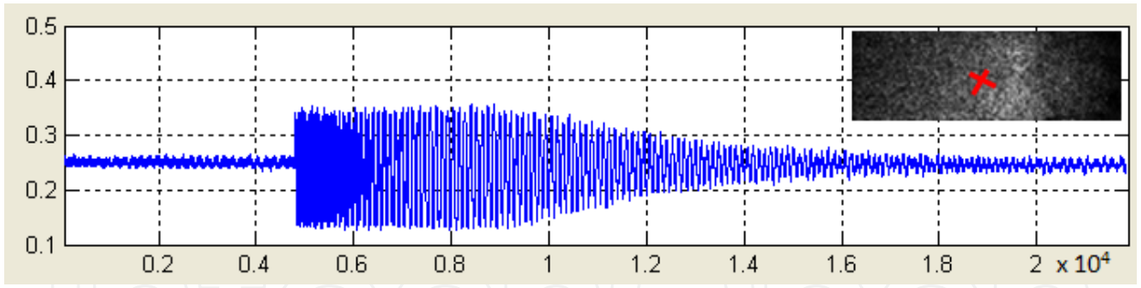

Fig. 16. Temporal history of a randomly chosen pixel, sampled at 15600 images/ second

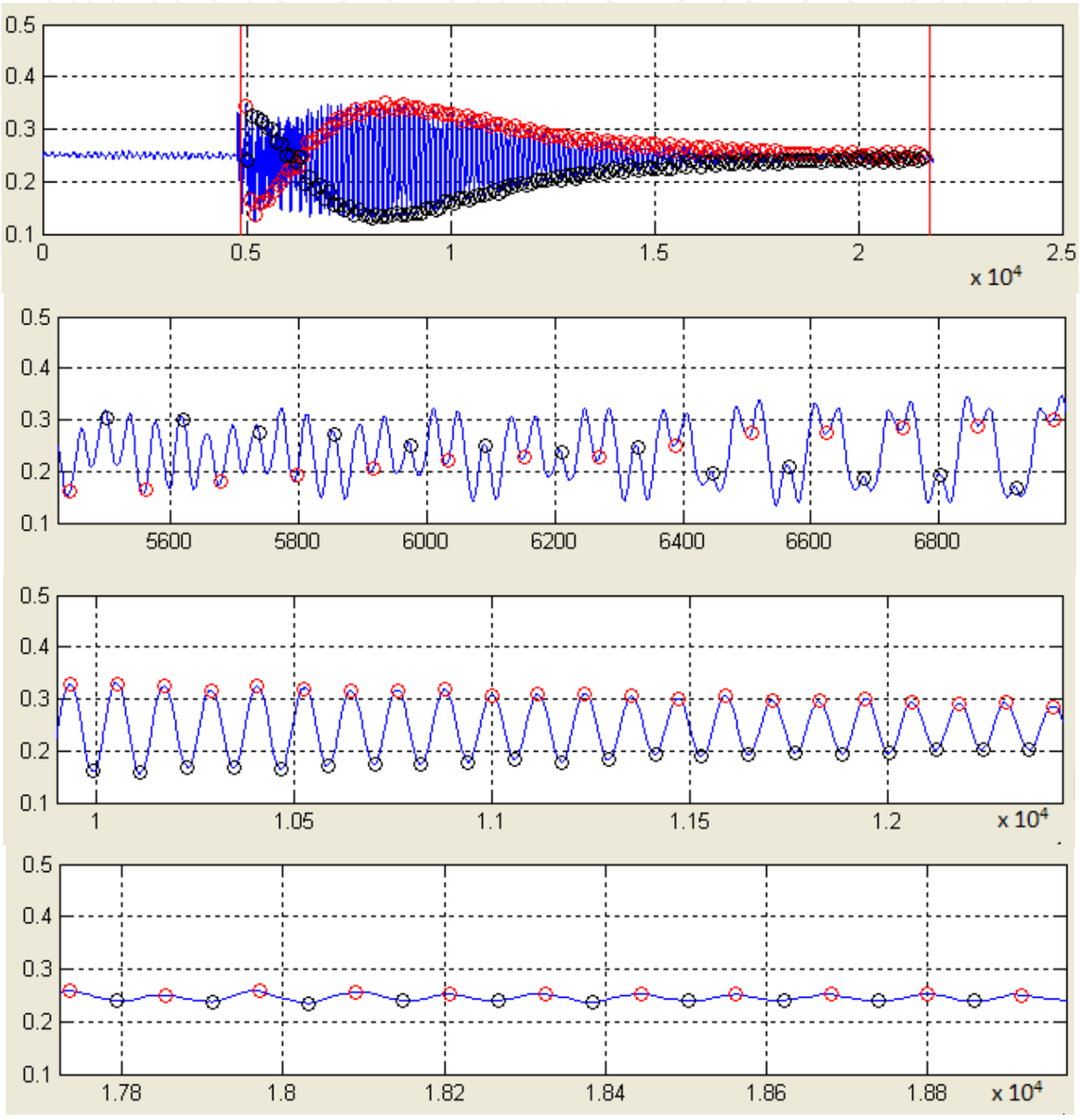

Fig. 17. Minima and maxima for each period of the damped temporal history for the chosen pixel

The frequency (or the period) is found after filtering the signal, fitting a sine function and finding, by an automatic procedure, its extrema (fig. 17) for any period considered. It may also be found by using the Fourier transform (fig. 18 a) of the signal corresponding to the free oscillations following the shock. The values for the period found by the two methods, expressed in number of images acquired at a rate of 15600 frames/ second, are very close, 118.1 in the first case and 117.9 in the second. It corresponds to a frequency of about 132 Hz. The damping may be calculated either by Fourier transform followed by a minimum-search fit or by fitting exponentials to the envelopes of the signal, shown in fig. 18 b. The values found by the different methods are also very close, 0.00545 for the first method and between 0.0051 and 0.0057 for the second.

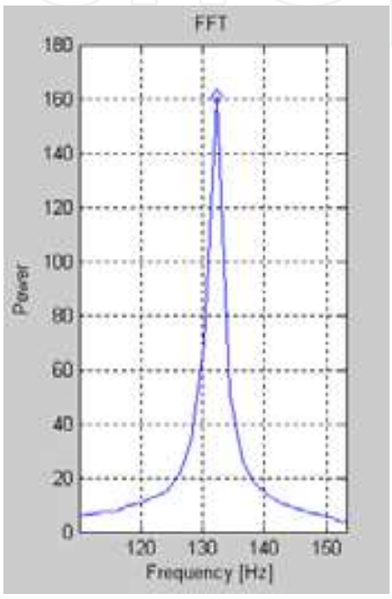

Fig. 18. (a) Frequency of the damped vibration found by FFT

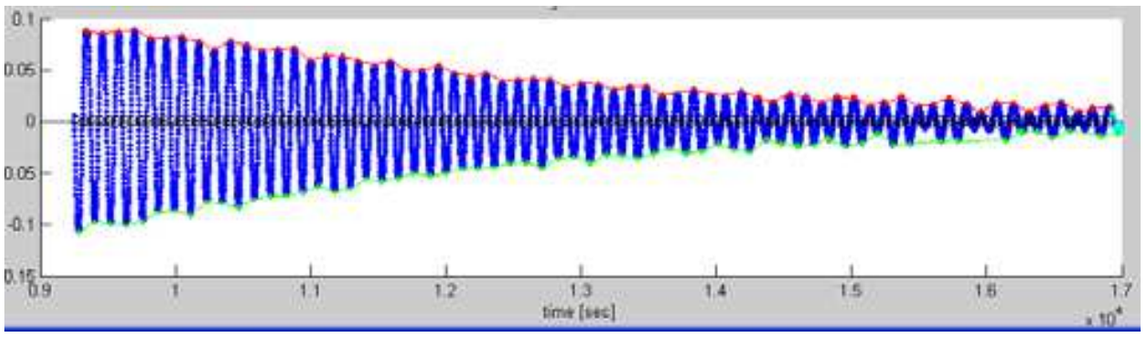

Fig. 18. (b) Envelopes of the free vibration for the considered pixel

6.2 Object in forced sinusoidal vibration: 2- and 4- step phase stepping

The measurements were made by acquiring 111 x 41 pixels wide correlograms at the rate of 26000 frames/ second, with four-step phase stepping. The correlograms were then treated in two different ways, either as "classical" 4-step phase-shifted images (6500 interferograms/ second), or as 2-step phase-shifted images (13000 interferograms/ second).

In both cases, the calculated interferograms used two quadrature fields recorded either with the object at rest, or with the object in vibration.
For the 2-step case, one period of object vibration at 142 Hz was sampled by 93 full-field interferograms at equal time intervals.
The acquired data allow obtaining, at that rate, considering 2-step phase stepping, the following results:

- The wrapped phase differences between the reference state and the state corresponding to any of the 93 sampling instants (fig. 19);

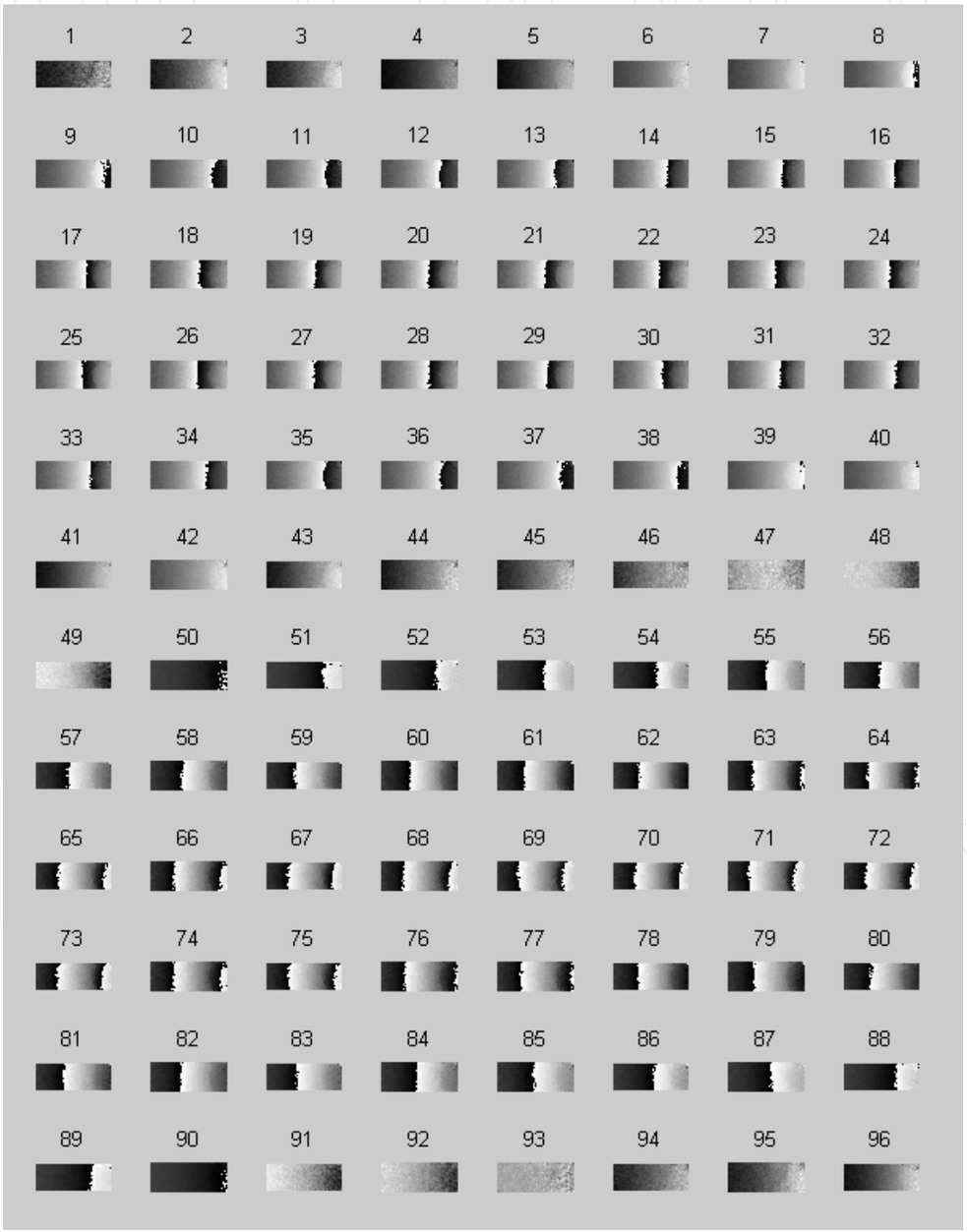

Fig. 19. Temporal history of full-field wrapped vibration amplitude fields

- The unwrapped phase differences between the reference state and the state corresponding to any of the 93 sampling instants (fig. 20);

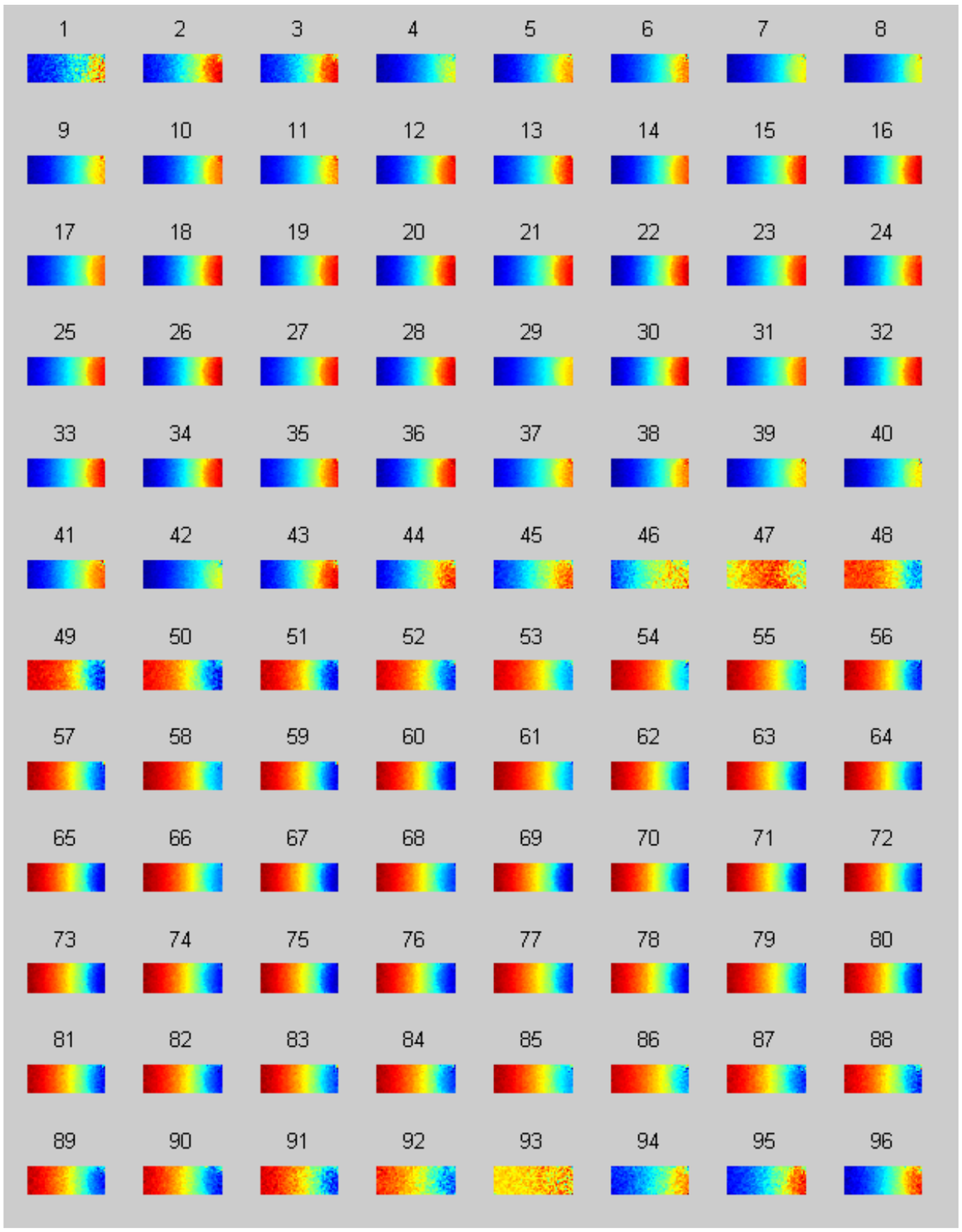

Fig. 20. Temporal history of full-field unwrapped vibration amplitude fields

- The unwrapped phase differences between any pair of phases corresponding to any of the 93 sampling instants (fig. 21);
- As a particular case, the phase differences around the zero-crossing and the extrema of a reference signal (the force signal), allowing to compute the complex frequency response, as mentioned at §3.2 and necessary for experimental modal analysis;

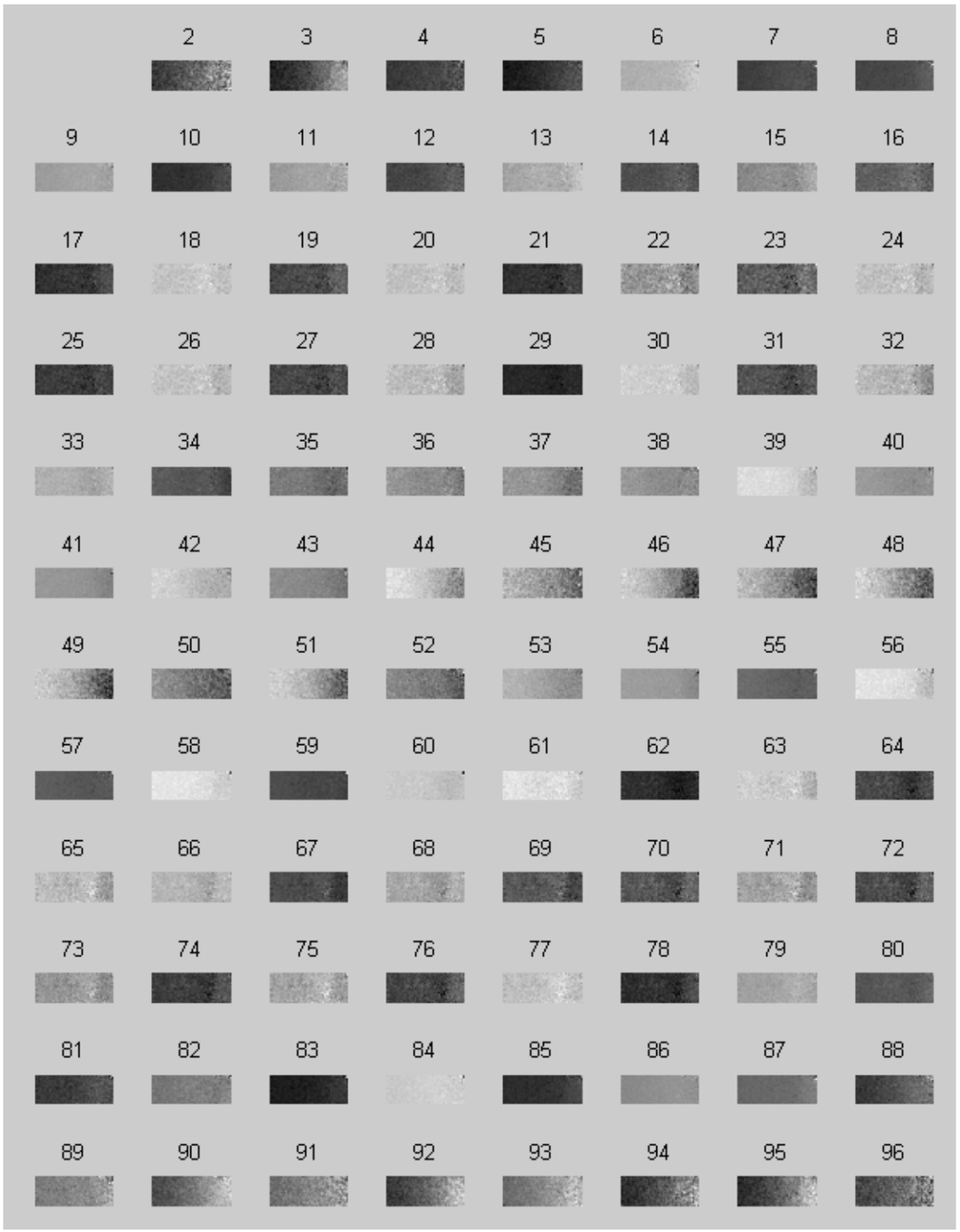

Fig. 21. Temporal history of full-field differences of unwrapped amplitude fields (or temporal history of object velocities)

- By integration during arbitrary time intervals, the full-field time-averaged holograms and the high-resolution time-average holograms (fig. 22).

Just as a remainder that these temporal histories have been recorded to resolve an harmonic vibration by a full-field interferometry system, by computing the sum of the interferograms noted from 1 to 93 in fig. 20, we may obtain either the "classical" time-average hologram in the upper part of fig. 22 or the high-spatial resolution time-average hologram in the lower part of fig. 22.

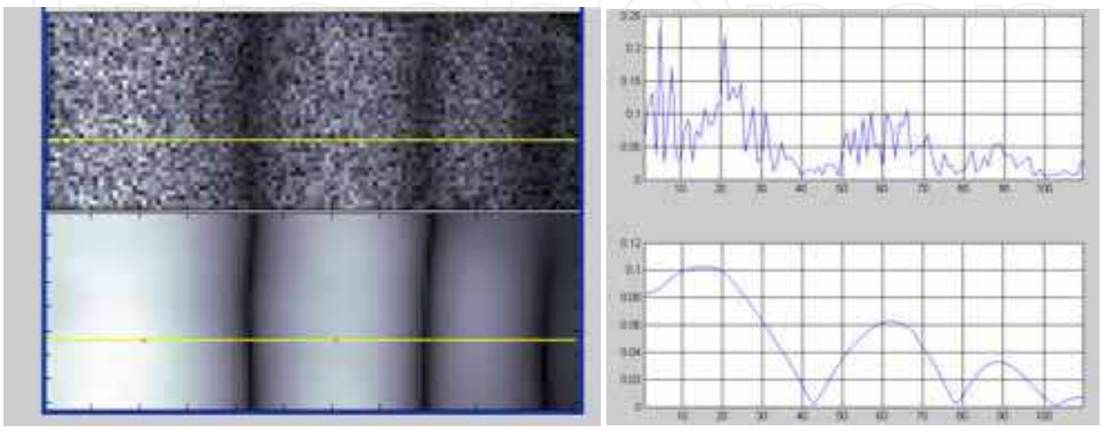

Fig. 22. Time-average and high-resolution time-average hologram during a vibration period

6.3 Object subjected to a variable force of arbitrary waveform; 2- and 4- step phase stepping

The object was perturbed with an arbitrary signal of which one period is shown in Fig. 23 (left) applied to a piezoelectric actuator. The measurements were made at a rate of 26000 images/ second, in the same conditions as those in § 6.2. At right is presented the unwrapped (upper plot) and wrapped (lower plot) temporal history of a randomly chosen pixel from the series of 5000 interferograms. It represents the deflection of that point between the two moments indicated at left (START, END).

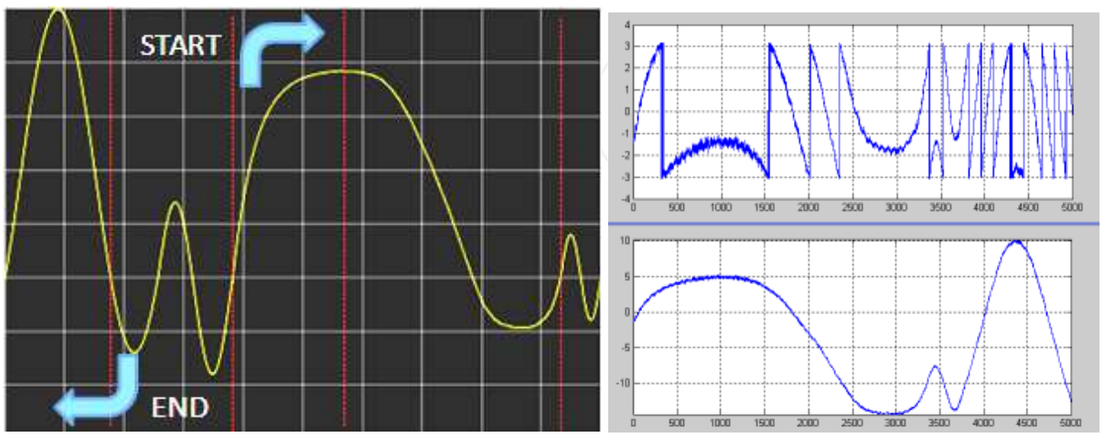

Fig. 23. One period of the force of arbitrary waveform applied by the piezoelectric actuator to the object (left) and the temporal history of a randomly selected pixel in the 5000 interferograms (right)

Such time histories as the one shown in fig. 23 (right) can be obtained for any of the 111 x 41 pixels of the 5000 interferograms. A few, randomly selected interferograms, are presented as wrapped phase patterns in fig. 24.

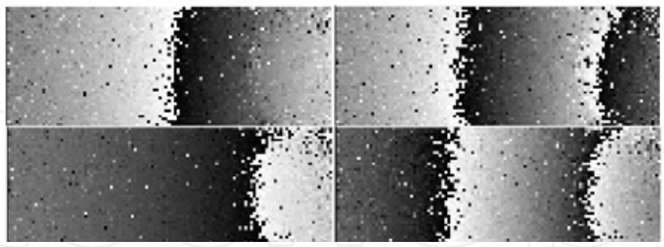

Fig. 24. A few randomly selected interferograms sampling the variable object deformation

7. Conclusions

Speckle interferometry has not stopped developing, in order to overcome its limitations. Important progress has been made towards higher temporal resolution measurements so as to give an adequate answer to the complex problems existing in vibration measurement and in vibracoustics. Higher spatial resolution has also been obtained in spite of the additive and multiplicative noise that covers the interferometric signal.
Many valuable results have been already obtained, and much work still have to be done in the algorithmics and data processing. New challenges appear, related to the manipulation and storage of massive data blocks characterizing high-rate multipoint temporal histories.

8. References

Aguanno, M.V., Lakestani, F., Whelan, M.P., Connelly, M.J. (2003). Single pixel carrier based approach for full field laser interferometry using a CMOS-DSP camera, Proc. SPIE 5251-5242, 304-312, ISSN 0277-786X

Asundi, A. & Singh, V. (2006). Amplitude and phase analysis in digital dynamic Holography, Optics Letters, Vol. 31, 16, 00-01, ISSN 0146-9592

Butters, J.N. & Leendertz, J. A. (1971). Holographic and video techniques applied to engineering measurement, *J Meas. Control*, 4, 349–354, ISSN: 0142-3312

Borza, D.N. (2000). Stepped-amplitude modulation interferometry a new real-time mechanical vibrations measurement technique, in: Interferometry in Speckle Light, Ed. Jacquot, P., Fournier, J-M., 305-310, Springer, ISBN 3-540-67943, Berlin – Heidelberg, ISBN: 3-540-67943-X

Borza, D.N. (2002). A New Interferometric Method for Vibration Measurement by Electronic Holography, Experimental Mechanics, 42, 4, 1-7, ISSN: 0014-4851

Borza, D.N. (2004). High-resolution time-average electronic holography for vibration measurement, Opt. Lasers Eng., 41, 415-527, ISSN 0143-8166

Borza, D.N. (2005). Mechanical vibration measurement by high-resolution time-averaged digital holography, Meas. Sci. Technol. 16, 1853–1864, ISSN: 0957-0233

Borza, D.N. (2008). Speckle Noise Reduction in Vibration Measurement by Time-average Speckle Interferometry and Digital Holography – a Unifying Approach, Journal of Solid Mechanics and Materials Engineering, 2, 6, 695-706, ISSN:1880-9871

Borza, D.N. (2006). Full-field vibration amplitude recovery from high-resolution time-averaged speckle interferograms and digital holograms by regional inverting of the Bessel function, Opt. Lasers Eng., 44, 747-770, ISSN: 0143-8166

Creath, K. (1985). Phase-shifting speckle interferometry, Appl. Opt., Vol. 24, No. 18, 3053-3058, ISSN: 0003-6935

Creath, K. & Slettemoen, G. (1985). Vibration-observation techniques for digital speckle-pattern Interferometry, J. Opt. Soc. Am. A, Vol. 2, No. 10, 1629-1636, ISSN 1084-7529

Doval, A.F. (2000). A systematic approach to TV holography, Meas. Sci. Tech., 11, R1-R36, ISSN: 0957-0233

Høgmoen, K. & Løkberg, O.J (1977). 1Detection and measurement of small vibrations using electronic speckle pattern interferometry, Appl. Opt. 16, 1869–75, ISSN: 0003-6935

Jacquot, P. (2008). Speckle interferometry: A review of the principal methods in use for experimental mechanics applications, Strain, 44, 57-69, ISSN 0039-2103

Joenathan, C. (1991). Vibration fringes by phase stepping on an electronic speckle pattern interferometer: an analysis, *Appl. Opt*. 30, 4658–4665, ISSN: 0003-6935

Kaufmann, G. (2003). Phase measurement in temporal speckle pattern interferometry using the Fourier transform method with and without a temporal carrier, *Opt. Comm.*, 217, 141-149, ISSN: 0030-4018

Moreau, A., Borza, D.N. & Nistea, I. (2008). Full-field vibration measurement by time-average speckle interferometry and by Doppler vibrometry – A comparison, Strain, 44, 386-397, ISSN: 0039-2103

Nistea, I. (2010). *Développement des techniques optiques et acoustiques de mesure de champs orientées vers la vibroacoustique*, PhD Thesis, Institut National des Sciences Appliquées de Rouen, France

Nistea, I. & Borza, D.N. (2010a). Experimental Analysis Of Failure In Embedded Electronics And Mechatronical Systems Under Thermal Stress, *Proceedings of IEEE-TTTC International Conference on Automation, Quality and Testing, Robotics*, May 28-30, 2010 Cluj Napoca, Romania, ISBN: 978-1-4244-6722-8

Nistea, I. & Borza, D.N. (2010b). Vibration measurement by Speckle Interferometry between high spatial and high temporal resolution, *Proceedings of Colloque francophone "Mesures et Techniques Optiques pour l'Industrie"* – SFO, CMOI, Toulouse (accepted)

Nakadate, S., Yatagai, T., & Saito, H. (1980). Digital speckle-pattern shearing interferometry, Applied Optics 19, 24, 4241-4246, ISSN: 0003-6935

Picart, P., Leval, J., Mounier, D. & Gougeon, S. (2005). Some opportunities for vibration analysis with time averaging in digital Fresnel holography Appl. Opt. 44, 337–43, ISSN: 0003-6935

Pryputniewicz, R.J. & Stetson, K.A. (1989). Measurement of vibration patterns using electro-optic holography. Proc SPIE, 1162, 456–67, ISSN 0277-786X

Singh V., Miao J., Wang, Z., Hegde, G. & Asundi, A. (2007). Dynamic characterization of MEMS diaphragm using time averaged in-line digital holography, *Optics Communications* 280, 285–290, ISSN: 0030-4018

Valera, J., Jones, J, Løkberg, O., Buckberry, C. & Towers, D. (1997). Bi-modal vibration analysis with stroboscopic heterodyned ESPI, *Meas. Sci. Technol.*, 8, 648–655, ISSN: 0957-0233

Van der Auweraer H., Steinbichler, H., Vanlanduit, S., Haberstok, C., Freymann, R., Storer, D. & Linet, V. (2002). Application of stroboscopic and pulsed-laser electronic speckle pattern interferometry (ESPI) to modal analysis problems, *Meas. Sci. Technol.*, 13, 451–463, ISSN: 0957-0233

Holography, Research and Technologies

Edited by Prof. Joseph Rosen

ISBN 978-953-307-227-2
Hard cover, 454 pages
Publisher InTech
Published online 28, February, 2011
Published in print edition February, 2011

Holography has recently become a field of much interest because of the many new applications implemented by various holographic techniques. This book is a collection of 22 excellent chapters written by various experts, and it covers various aspects of holography. The chapters of the book are organized in six sections, starting with theory, continuing with materials, techniques, applications as well as digital algorithms, and finally ending with non-optical holograms. The book contains recent outputs from researches belonging to different research groups worldwide, providing a rich diversity of approaches to the topic of holography.

How to reference

In order to correctly reference this scholarly work, feel free to copy and paste the following:

Dan Nicolae Borza (2011). Vibration Measurement by Speckle Interferometry between High Spatial and High Temporal Resolution, Holography, Research and Technologies, Prof. Joseph Rosen (Ed.), ISBN: 978-953-307-227-2, InTech, Available from: http://www.intechopen.com/books/holography-research-and-technologies/vibration-measurement-by-speckle-interferometry-between-high-spatial-and-high-temporal-resolution

INTECH
open science | open minds

InTech Europe
University Campus STeP Ri
Slavka Krautzeka 83/A
51000 Rijeka, Croatia
Phone: +385 (51) 770 447
Fax: +385 (51) 686 166
www.intechopen.com

InTech China
Unit 405, Office Block, Hotel Equatorial Shanghai
No.65, Yan An Road (West), Shanghai, 200040, China
中国上海市延安西路65号上海国际贵都大饭店办公楼405单元
Phone: +86-21-62489820
Fax: +86-21-62489821

IntechOpen